Droplet Evaporation under High Pressure and Temperature Conditions: A Comparison of Experimental Estimations and Direct Numerical Simulations

C. Steinhausen[1]*, J. Reutzsch[1], G. Lamanna[1], B. Weigand[1],
R. Stierle[2], J. Gross[2],
A. Preusche[3], A. Dreizler[3]

[1]Institute of Aerospace Thermodynamics, University of Stuttgart, Germany
[2]Institute for Thermodynamics and Thermal Process Engineering, University of Stuttgart, Germany
[3]Institute of Reactive Flows and Diagnostics, Technical University of Darmstadt, Germany
*Corresponding author: christoph.steinhausen@itlr.uni-stuttgart.de

Abstract
Droplet evaporation within combustion chambers is of high importance for stable and efficient combustion. For ambient pressures exceeding the critical pressure of the injected fuel, evaporation processes are not fully understood yet. Especially the temperature evolution of the injected fuel is a key parameter to understand the transition of near critical droplet evaporation to dense fluid mixing. Hence, this study shows various approaches to investigate the temperature evolution of alkane droplets in a nitrogen atmosphere under high temperature and pressure conditions. First, we present a direct numerical simulation of a levitated alkane droplet and compare it with two different analytical evaporation models. The latter are the non-equilibrium models by Gyamarthy [1] as well as Young [2]. The simulation of a levitated droplet is performed with the multiphase solver FS3D. For that, the implemented evaporation models are adapted and extended to account for stable simulations in high pressure and temperature regimes. Based on these insights the vapour concentration in the wake of a free falling droplet is investigated with FS3D and collated with experimental Raman scattering results. Finally, the temperature profile gained from the direct numerical simulation in the wake of the free falling droplet is compared to a re-evaluation of the Raman scattering results. This re-evaluation is based on the PC-SAFT equation of state and an adiabatic mixing assumption.

Keywords
high pressure and temperature condition; droplet evaporation; direct numerical simulation

Introduction

Droplet evaporation within combustion chambers is of high importance for a stable and efficient combustion. Especially for high pressures exceeding the critical value of the injected fluids, mixing and evaporation processes as well as fundamental changes in fluid behaviour are not fully understood yet. The latter have received increased attention in the past decade, as the recently published literature shows [3, 4, 5, 6, 7]. Since the main objectives are evaporation and disintegration processes of liquid fuel at pressures and temperatures either close to or exceeding the critical point of the injected fuels, temperature evolution of the injected fluid has become a research concern with increasing interest recently [8, 9, 10]. Microscopic investigations by Santoro and Gorelli [11], Simeoni et al. [12] as well as Bencivenga et al. [13] made it possible to distinguish different regions above the critical pressure. Regions with subcritical temperature and supercritical pressure show a liquid-like behaviour whereas regions with high supercritical temperatures, which are on the right of the Widom line, which is characterised by the maxima in specific isobaric heat capacity, are gas-like. The area between the critical isotherm and the Widom line can be characterized as the supercritical region. In this region fluids behave either liquid or gas-like. Besides this distinction a continuous fluid behaviour is experienced crossing the critical isotherm and Widom line. Since the critical isotherm as well as the Widom line are both a function of temperature, the study of the fluid temperature is, besides the speed of sound, the heat transfer processes and the relaxation behaviour of the fluids, one of the key parameters to enable macroscopic investigations of these different fluid behaviours.
Besides the aforementioned microscopic investigations different thermodynamic models have been introduced to understand and predict the transition from evaporation to dense fluid mixing [14, 15]. One common assumption of these thermodynamic prediction models is the assumption of global thermodynamic equilibrium. The latter only uses the initial temperature and pressure of fluid and environment as input parameters to calculate adiabatic mixing temperatures with respect to concentrations. By finding the intersection of the adiabatic mixing line and the vapour liquid equilibrium, the surface temperature is estimated. Lamanna et al. [10] discussed the validity of this global equilibrium assumption recently. They concluded that a non-equilibrium framework rather than a global equilibrium assumption might be better suited to estimate surface temperatures in heterogeneous media. However, quantitative temperature data for validation of the non-equilibrium analytical framework is rare. Bork [16] used spontaneous Raman-scattering to investigate the concentration field as well as the relative number density in the wake of a free falling acetone, n-hexane, n-heptane, diethyl-ether, and FK-5-1-12 droplets in a nitrogen environment at high pressure and temperature conditions. The Raman scattering results of an nearcritical, free falling n-heptane droplet

were presented by Bork et al. [8]. Based on the data of Bork et al. [8], Steinhausen et al. [9] estimated a droplet surface temperature using a local thermodynamic equilibrium assumption and the perturbed-chain statistical associating fluid theory (PC-SAFT) equation of state (EoS) [17]. Since a validation of non-equilibrium frameworks using the estimation of Bork et al. [8] and Steinhausen et al. [9] might be theoretically possible, the lack of quantitative data proves to be the biggest obstacle. However, further comparison of the local thermodynamic equilibrium assumption as well as the non-equilibrium frameworks with numerical data is possible. This study shows three different approaches to investigate the temperature evolution of a n-hexane droplet in a nitrogen atmosphere with high temperature and pressure conditions. First, we present a direct numerical simulation performed with the multiphase solver Free Surface 3D (FS3D) of a levitated droplet and compare it with two analytical evaporation models. Finally, the temperature profile gained from the direct numerical simulation in the wake of the free falling droplet is compared to a re-evaluation of the spontaneous Raman-scattering results.

Methodology

The temperature evolution of the vapour-liquid interface is essential for evaporation processes, like the transition from sub- to supercritical fluid state. The following section provides a brief overview of the methodology used in the presented work to estimate mixing temperatures based on a local adiabatic mixing assumption using relative number density and concentration in the wake of the droplet. The latter are both measured using spontaneous Raman-scattering. Additionally, the evaporation models used for temperature and interface evolution are summarized.

Experimental setup and data evaluation

The methodology and experimental setup, which provides a constant far-field concentration, used for the spontaneous Raman-scattering investigations is described in Bork et al. [8]. Based on the local relative number density and concentration data in the wake of the droplet, the concentration-temperature field in the wake is estimated using the PC-SAFT EoS [17] together with a local adiabatic mixing assumption. To extrapolate the temperature-concentration data to the vapour-liquid equilibrium (VLE), a mathematical fit based on the PC-SAFT EoS and a global adiabatic mixing assumption is generated by adjusting the temperature of the liquid, while holding the temperature of the solvent and pressure constant. A detailed description of the local adiabatic mixing assumption used to evaluate the temperature field in the wake of the droplet as well as the estimation of this extrapolated Raman temperature can be found in Lamanna et al. [10].

Selection of evaporation models

Two similar evaporation models are chosen to estimate the temperature evolution of the interface for a droplet in a high pressure and temperature environment. Namely, the evaporation model of Gyarmathy [1] and the model of Young [2] are selected. Thermodynamic properties of the pure components are extracted from NIST Database [18], whereas the thermodynamic properties of the mixtures are computed according to Amagats law [19] for gas mixtures. The calculation of the diffusion coefficients are based on the Wilke and Lee [20] model. The Lennard-Jones parameter for n-hexane and nitrogen are extracted from the NIST Database [18]. When considering solubility effects, the saturation pressure of the liquid in the vapour phase is corrected by the binary mixture composition in equilibrium using an enhancement factor as explained by Luijten [21]. To match the experimental Raman scattering results the initial droplet diameter is set iteratively, so that the diameter at $t = 0.5$ s is in the range of $D_{t=0.5\mathrm{s}} = 1.25 \pm 0.2$ mm. The main differences between the model assumptions are the following:

- **Gyarmathy:** The evaporation model of Gyarmathy [1] is a Langmuir type model assuming a collision free zone around the drop and a continuum approach in the far-field of the drop. Inside this zone a half-Maxwellian velocity distribution is used to describe the incoming vapour molecules. Therefore, the coupling conditions at the interface are of quasi-equilibrium.
- **Young:** The evaporation model of Young [2] is a Langmuir type model following Onsager's theory. In the collision free zone a Grad velocity distribution is utilised to model the incoming vapour molecules. Hence, the coupling conditions at the interface accounts for non-equilibrium conditions. The Young model is valid within the Onsager linear region.

Both evaporation models neglect heat conduction within the liquid phase, which leads to a spatially constant droplet temperature. Hence, the temperature of the liquid phase equals the droplets surface temperature. For a comprehensive discussion regarding the selection of evaporation models as well as the modelling of the interfacial fluxes the reader is referred to Lamanna et al. [10]. The importance of non-equilibrium models in temperature evolution of high pressure flows is highlited in the work of Lamanna et al. [10]. The accuracy of the evaporation model is assessed with an extrapolated Raman temperature.

Numerics

This section comprises the numerical fundamentals and the setup of the two conducted simulations. For the numerical simulations we use the multiphase software package FS3D. A short description of the used methods will be given in the following.

Fundamentals

The multiphase DNS solver FS3D has been developed at the Institute of Aerospace Thermodynamics in Stuttgart. The code is well validated and a large number of physical processes have been investigated in the last twenty years. Among them are droplet deformations [22], droplet-film interactions [23], droplet-wall interactions [24] and droplet collisions [25]. In addition, heat and mass transfer is included, which allows simulations with phase change. A wide variety of studies has been performed comprising evaporating droplets [26, 27], droplets under extreme ambient conditions [28], spray atomization with evaporation [29], or also liquid solid phase change problems [30]. An detailed overview of FS3D can be found in [31].

FS3D solves the incompressible Navier-Stokes equation for mass and momentum as well as the energy conservation. They are discretised using a finite volume method and a Marker and Cell grid [32]. Thus, scalars are stored at the cell centres, velocities at the cell faces, respectively. The conservation equations are given by

$$\rho_t + \nabla \cdot (\rho u) = 0, \tag{1}$$

$$(\rho u)_t + \nabla \cdot [(\rho u) \otimes u] = \nabla \cdot (S - Ip) + \rho g + f_\gamma, \tag{2}$$

$$(\rho c_p T)_t + \nabla \cdot (\rho c_p T u) = \nabla \cdot (k \nabla T) + T_0 \left[(\rho c_p)_t + \nabla \cdot (\rho c_p u)\right] + \Delta h_v \dot{m}''', \tag{3}$$

where ρ represents the density, u the velocity, p the static pressure, g the gravitational forces and f_γ body forces. The latter is used to model surface tension in the vicinity of the interface. Three different models are implemented to compute the surface tension. They are the conservative continuous surface stress model by Lafaurie et al. [33], the continuum surface force model by Brackbill et al. [34], as well as the balanced force approach by Popinet [35], which is the one used in this study. The viscous stress tensor S is defined by $S = \mu \left[\nabla u + (\nabla u)^T\right]$ for Newtonian fluids with μ the dynamic viscosity. Concerning the energy equation (3), c_p is the specific heat capacity, T the temperature, T_0 the reference temperature at zero enthalpy, k the heat conductivity, Δh_v the latent heat of vaporization and $\dot{m}'''$ the volumetric mass source of vapour.

FS3D uses the Volume of Fluid (VOF) method developed by Hirt and Nichols [36], therefore, we introduce additional field variables f_i. They represent the amount of liquid ($i = 1$), vapour ($i = 2$) and solid ($i = 3$). f_1 is defined as

$$f_1(x,t) = \begin{cases} 0 & \text{gaseous phase} \\ ]0;1[& \text{at the interface} \\ 1 & \text{liquid phase.} \end{cases} \tag{4}$$

f_2 represents the volume fraction of the vapour phase. In this paper we consider only liquid, gas and vapour, what leads to the two used transport equations of both VOF-variables:

$$(f_1)_t + \nabla \cdot (f_1 u_\Gamma) = -\dot{m}'''/\rho_l \tag{5}$$

$$(f_2)_t + \nabla \cdot (f_2 u_{gp}) = \nabla \cdot (\mathcal{D}_{\text{bin}} \nabla f_2) + \dot{m}'''/\rho_v \,. \tag{6}$$

ρ_l and ρ_v are the liquid and vapour density and $\mathcal{D}_{\text{bin}}$ represents the binary diffusion coefficient. Due to the volume generation inherent to evaporation the velocities at the interfaces u_Γ and u_{gp} differ. Based on the one-field-formulation of the VOF-method, the local fluid properties are calculated with the volume fractions. Hence, the local viscosity reads

$$\mu(x,T,t) = \mu_l(T) f_1(x,t) + \mu_v(T) f_2(x,t) + (1 - f_1(x,t) - f_2(x,t)) \mu_g(T) \,. \tag{7}$$

The volumetric mass source of vapour $\dot{m}'''$, which is only present at the interface, is dependent on the local density, the diffusion coefficient and the local gradient of vapour mass fraction X_v. In a first step the local area specific mass source of vapour

$$\dot{m}'' = \frac{\mathcal{D}_{\text{bin}} \rho_{gp}}{1 - f_1} \nabla X_v \hat{n}_\Gamma \tag{8}$$

is calculated and then multiplied by the local interface density a_Γ in order to obtain the volumetric mass source. Further, we assume saturation conditions at the local interfaces. Thus, the vapour pressure is the saturation pressure, which is estimated with the Wagner equation. As discussed in Lamanna et al. [10] this assumption is justified for millimetre sized droplets ($D_d > 1000\ \mu\text{m}$), because the interfacial temperature and vapour pressure jumps are negligible. For further details on Wager equation we refer to Schlottke [37].

Numerical setup

In this section we describe the numerical setups of two simulations. A levitated droplet (case 1) on the one hand and a falling drooplet (case 2) on the other hand, which is adapted from the experimental test rig. Both simulations are performed on a three-dimensional regular grid. The liquid of the droplets is n-hexane and the surrounding gas is nitrogen. The material properties are taken from the same sources described in the previous section. Case 1 is implemented with a a cubic domain with a resolution of 256^3 cells. The droplet is initialized as a sphere, positioned at the centre of the domain. Similar to the analytic procedure mentioned before the diameter is set in a way, that it reaches the final diameter $d_{\text{case1,fin}} = 1.25$ mm after 0.5 s. The distance to all sides, which are set as continuous Neumann-boundaries, is $2d_{\text{case1}}$. The temperatures of the liquid and the gaseous phase is set to $T_{\text{case1}} = 473.15$ K.

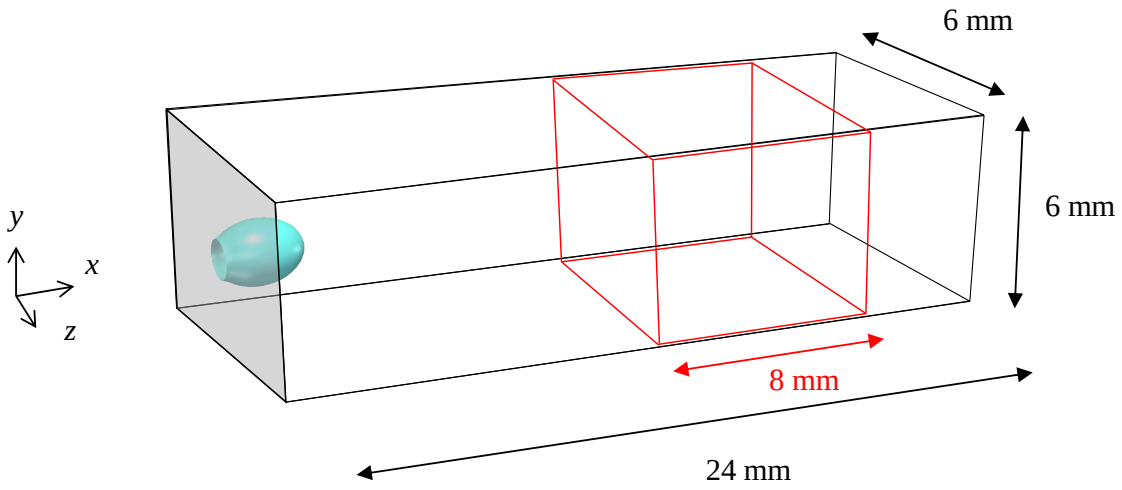

Figure 1. Sketch of the numerical setup of the falling droplet of case 2.

The numerical setup of case 2 is shown in figure 1. The dimensions are derived from the used experimental test rig; the resolution of the simulation is 512x128x128 cells. Note, that to reduce computational costs the squared base was reduced from 8x8 mm² to 6x6 mm², since the amount of vapour in the outer regions is negligible. The droplet is initialised as an ellipsoid, which is "cut" at the top, where a no slip wall boundary condition is applied. It has a small initial speed in x-direction. Previous studies have shown, that this setup describes the falling behaviour of the droplet best. This includes oscillation behaviour, droplet shape characteristics and velocity during falling as well as we'll see later, the vapour field distribution in the wake of the droplet. The other boundaries are all set to continuous ones. The red cuboid in figure 1 represents the measurement part in the wake of the droplet from which the values of the vapour field distribution are taken.

Results and discussion

The presented cases in this work are twofold. A numerical investigation using FS3D of a free falling n-hexane droplet in a nitrogen atmosphere under equal conditions is compared to the measured concentration field as well as the estimated concentration-temperature field in the droplet wake from the spontaneous Raman-scattering investigations. Due to the characteristic dwell time of 0.5 s of the Raman-scattering investigations, which were conducted with a droplet detachment frequency of 2 Hz, the droplet temperature at detachment is unknown. Therefore, a heated, levitated n-hexane droplet in a nitrogen atmosphere under high pressure and temperature conditions is investigated at first using the presented evaporation models in the previous section. The temperature evolution of the droplet is compared to the numerical simulation of FS3D. The calculation time of 0.5 s is based on the before mentioned characteristic dwell time of the Raman-scattering investigations. The surface temperature of the droplet at $t = 0.5$ s from the evaporation model of Young with consideration of solubility effects is then used as an input parameter for the numerical simulation of the free falling droplet. The Young model with consideration of solubility was chosen, because it accounts for non-equilibrium conditions at the interface and considers the solubility of nitrogen into the droplet. As mentioned in the previous section, we will refer to the levitated droplet as case 1 and to the free falling droplet as case 2.

Evaporation of a levitated droplet under high pressure and temperature conditions (case 1)

The temperature evolution of a preheated, levitated n-hexane droplet with a initial fluid temperature of $T_{\text{fluid}} = 473.15$ K in a nitrogen atmosphere at $p_{\text{amb}} = 60$ bar and $T_{\text{amb}} = 473.15$ K is depicted in figure 2. Note, that the nitrogen concentration in the far field of the droplet is set to $x_{\infty,\text{N2}} = 0.9979$ and the initial droplet diameter is set iteratively to $D_{t=0.5\text{s}} = 1.25 \pm 0.2$ mm at $t = 0.5$ s, which are the values of the spontaneous Raman-scattering investigations. Figure 2 shows a similar temperature evolution for the models by Gyarmathy and Young. The consideration of solubility of gaseous nitrogen into the liquid n-hexane droplet leads to an enhanced evaporation

rate. Since the computations with solubility show a lower temperature as without solubility effects, consideration of solubility effects leads to the expected results. For the two evaporation models it is evident, that the droplet is rapidly cooling down and does not reach an equilibrium state during calculation time.

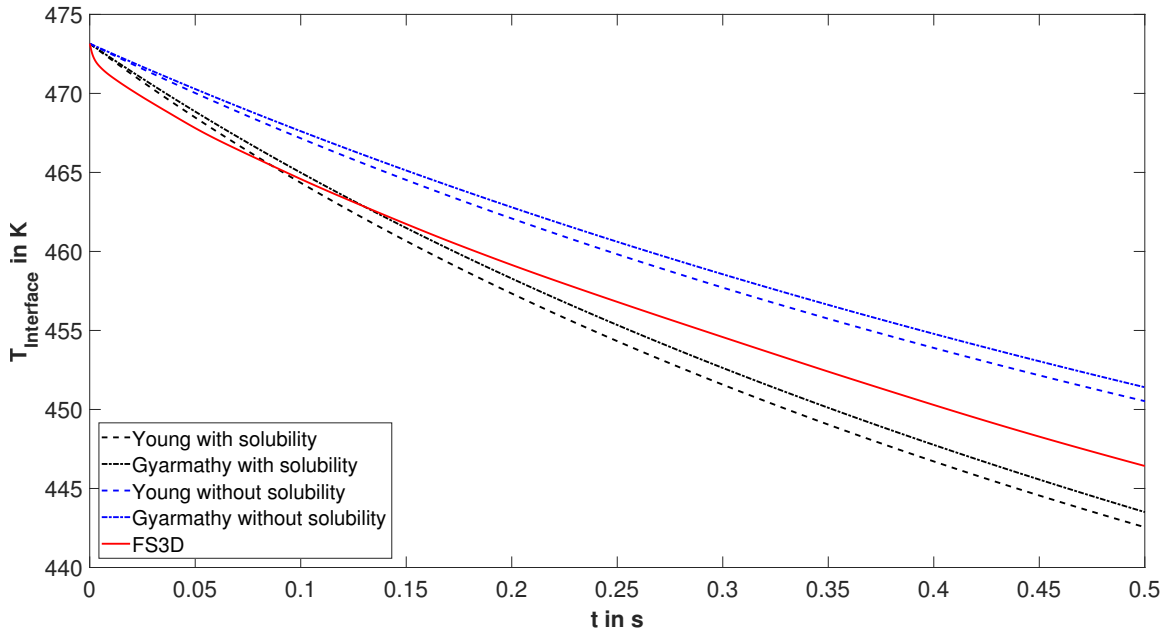

Figure 2. Surface temperature evolution of a preheated, levitated n-hexane droplet in a nitrogen atmosphere at $p_{\text{amb}} = 60$ bar, $T_{\text{amb}} = 473.15$ K, $T_{\text{fluid}} = 473.15$ K and $x_{\infty,\text{N2}} = 0.9979$. The initial droplet diameter is set iteratively, that the diameter at $t = 0.5$ s is in the range of $D_{t=0.5\text{s}} = 1.25 \pm 0.2$ mm. This matches the droplet diameter during the Raman scattering investigations.

The temperature evolution of the numerical simulation with FS3D shows a similar trend as the evaporation models. Due to numerical convergence problems at the beginning of the simulation the slope at early times differs from the analytical solutions. Concordantly, the slope differs slightly at later times as well. The overall trend of the numerical simulation shows a good agreement to the analytical models. Small deviations between the analytical solutions and the numerical simulation arise from the omission of solubility of nitrogen into the liquid phase. However, further validation is necessary to clearly support the importance of solubility effects as stated by Lamanna et al. [10]. Furthermore, for future investigations improved evaporation models for FS3D accounting for simulation under high pressure and temperature are under development.

Evaporation of a free falling droplet under high pressure and temperature conditions (case 2)

A qualitative comparison of the concentration field in the droplet wake of a free falling n-hexane droplet in a nitrogen atmosphere at $p_{\text{amb}} = 60$ bar, $T_{\text{amb}} = 473.15$ K and $x_{\infty,\text{N2}} = 0.9979$ is shown in figure 3. On the left hand side a single shot spontaneous Raman-scattering is depicted, on the right hand side the mid plane of the FS3D simulation is displayed. Note, that the fluid temperature in the droplet injector was set to $T_{\text{fluid}} = 473.15$ K during the experiments, whereas the initial droplet temperature for the simulation with FS3D was set to $T_{Droplet,0} = 440$ K to account for evaporation processes during the dwell time in the experiments of $t = 0.5$ s prior to the droplet detachment. Since the initial droplet temperature is one key parameter for the evaporation processes and the droplet temperature might be up to 30 K below the temperature measured in the droplet injector (figure 2), the consideration of the characteristic dwell time of the experiment is vital for the comparability of experimental and numerical investigations. Comparing the concentration field in the droplet wake leads to a reasonably good agreement, considering the statistical fluctuations out of the measurement plane due to turbulence in the droplet wake. Especially the Karman vortices in the droplet wake, which are dependent on the characteristic droplet oscillation, show a similar behaviour. This confirms the choice of the initial droplet setup used in the numerical simulation. In previous studies we compared time resolved shadowgraphy investigations of free falling n-pentane droplets in a nitrogen atmosphere at high pressure conditions with FS3D simulations. The evaluation of those have shown a good accordance of the droplet behaviour regarding velocity, oscillation frequency and droplet shape. For additional validation of the presented case, time resolved experiments would be an interesting extension.

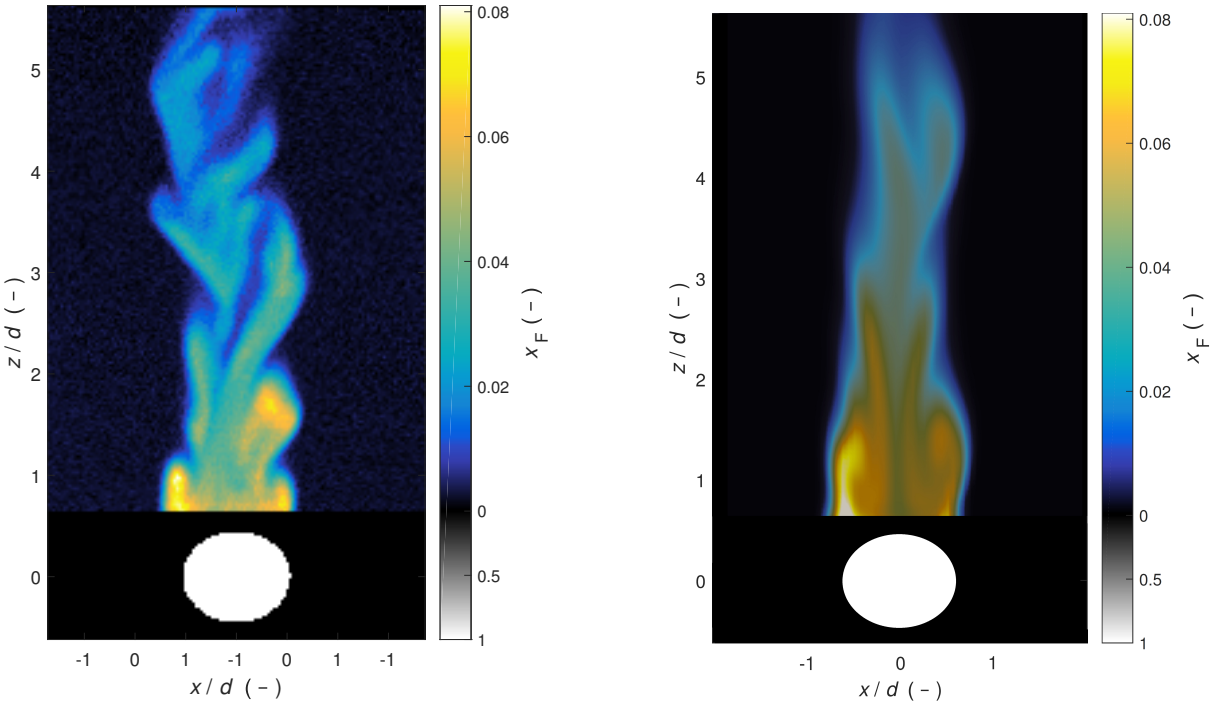

(a) Single shot spontaneous Raman-scattering results with colour scale for mole fraction.

(b) FS3D results with colour scale for mole fraction.

Figure 3. Concentration field in the droplet wake of a free falling n-hexane droplet in a nitrogen atmosphere at $p_{\text{amb}} = 60$ bar, $T_{\text{amb}} = 473.15$ K, $T_{\text{fluid}} = 473.15$ K and $x_{\infty,\text{N2}} = 0.9979$.

To investigate the concentration-temperature profile in the droplet wake, we extract the temperature and concentration in each cell of the measurement domain displayed in red in figure 1 from the numerical data. This data is plotted in red in the T,x-diagram shown in figure 4. Additionally, the estimated concentration-temperature data from the Raman-scattering investigation is displayed in black in the same diagram. Furthermore, the extrapolation of the experimentally estimated temperature field is shown as a black line and the vapour liquid equilibrium (VLE) is depicted as a blue line. The latter is computed using the PC-SAFT EoS.

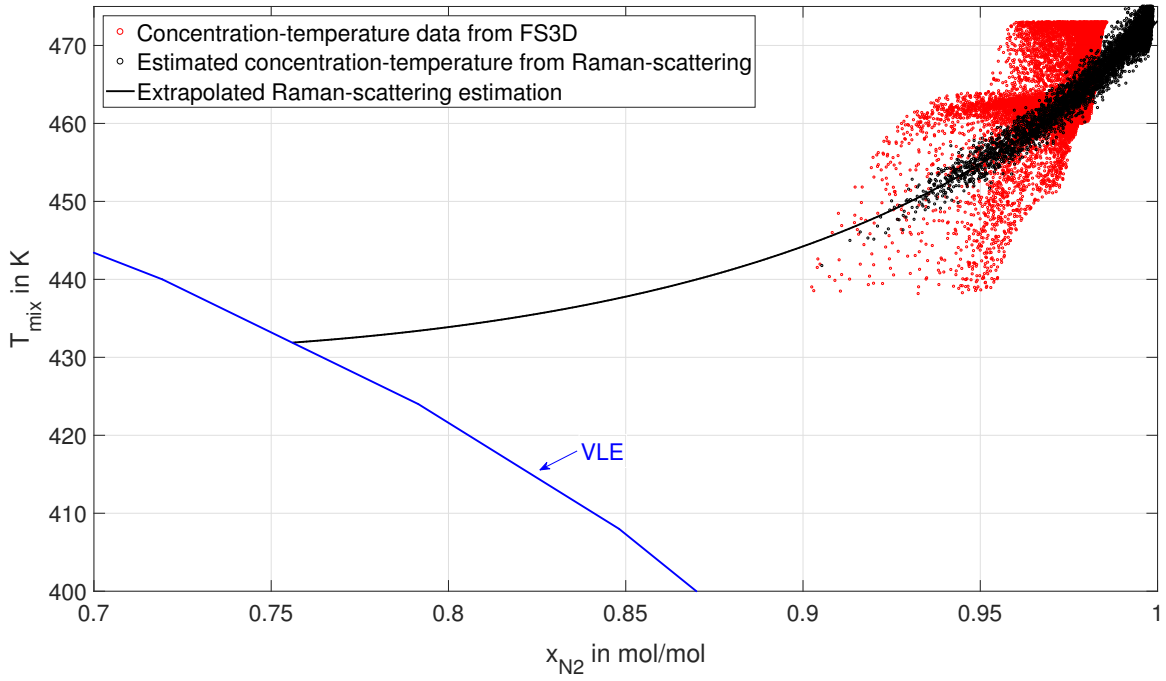

Figure 4. Comparison of experimental, numerical and theoretical concentration-temperature profiles; Black line: PC-SAFT-based fit to the experimental data; Blue line: vapour liquid equilibrium; Experimental and numerical conditions: $p_{\text{amb}} = 60$ bar, $T_{\text{amb}} = 473.15$ K; Test fluids: n-hexane in nitrogen, initial temperature $T_{\text{fluid}} = 473.15$ K, initial droplet diameter $D_{t=0.5\text{s}} = 1.25$ mm.

The comparison of the concentration-temperature data shows good agreement. Hence, the temperature estimation of the concentration data is supported by the numerical simulation. Note, that due to numerical diffusion in the vapour field, inaccuracies and the large number of data points, temperature values above 473 K are irrelevant for the comparison and hence not shown. The extrapolated Raman temperature at the vapour-liquid interface defined by Lamanna et al. [10], which is the intersection of the PC-SAFT based fit of the experimental data with the VLE, differs more than 10 K from the temperatures at $t = 0.5$ s gained from evaporation modelling shown in figure 2. Consequently, further validation of the used evaporation models as well as the local adiabatic mixing assumption used to estimate the temperature from the Raman-scattering measurements are vital. By virtue of this fact, the need of direct temperature measurements in the wake of the droplet as well as the droplet itself is indisputable.

Conclusions

A numerical and analytical study of droplet evaporation dynamics at high pressure and temperature conditions has been conducted. First, we used analytical non-equilibrium evaporation modelling and direct numerical simulation to investigate the temperature evolution of a levitated droplet. Secondly, the concentration-temperature field in the wake of a freely falling droplet was estimated from experimental concentration data based on a local equilibrium assumption and compared to a direct numerical simulation. All investigations were carried out on preheated n-hexane droplets in a nitrogen atmosphere at high pressure and temperature conditions. Our main conclusions are the following:

- The temperature evolution of the analytical evaporation models clearly show the influence of solubility effects under high pressure and temperature conditions. Furthermore, the numerical simulations show similar trends as analytical modelling.
- The used numerical method of FS3D is suitable for droplet evaporation under high pressure and temperature conditions. Nevertheless, for more precise results and future simulations an improved evaporation model is required.
- Validation of the numerical setup, the evaporation models, as well as the local adiabatic mixing assumption used to estimate the temperature from the Raman-scattering measurements are vital for future investigations. Therefore, quantitative temperature data of the droplet wake as well as the droplet surface is necessary.

Acknowledgements

The authors gratefully acknowledge the German Research Foundation (DFG) for the financial support through the collaborative research centre SFB-TRR75.

Nomenclature

D	diameter [m]
$\mathcal{D}_{\text{bin}}$	binary diffusion coefficient [m^2 s^{-1}]
c_p	specific heat capacity at constant pressure [J K^{-1} kg^{-1}]
f	VOF variable [-]
g	gravitational acceleration [m^{-2}]
h_v	specific latent heat of vaporization [J kg^{-1}]
k	heat conductivity [W m^{-1} K^{-1}]
$\dot{m}''$	area mass source [kg m^{-2} s^{-1}]
$\dot{m}'''$	volumetric mass source [kg m^{-3} s^{-1}]
p	pressure [Pa]
T	temperature [K]
t	time [s]
u	velocity [m s^{-1}]
x	mole fraction [-]
X_v	vapour mass fraction [-]
μ	viscosity [Pa s]
ρ	density [kg m^{-3}]
EoS	equation of state
FS3D	free surface 3D
NIST	National Institute of Standards and Technology
PC-SAFT	perturbed-chain statistical associating fluid theory
VLE	vapour-liquid equilibrium
VOF	volume of fluid

References

[1] Gyarmathy, G., *Multiphase Science and Technology*, Vol. 1, No. 1-4, 1982, pp. 99–279.
[2] Young, J. B., *International Journal of Heat and Mass Transfer*, Vol. 36, No. 11, 1993, pp. 2941–2956.
[3] Falgout, Z., Rahm, M., Sedarsky, D., and Linne, M., *Fuel*, Vol. 168, 2016, pp. 14–21.

[4] Müller, H., Niedermeier, C. A., Matheis, J., Pfitzner, M., and Hickel, S., *Physics of Fluids*, Vol. 28, No. 1, 2016, pp. 015102.
[5] Baab, S., Förster, F. J., Lamanna, G., and Weigand, B., *Experiments in Fluids*, Vol. 57, No. 11, 2016, pp. 3068.
[6] Crua, C., Manin, J., and Pickett, L. M., *Fuel*, Vol. 208, 2017, pp. 535–548.
[7] Baab, S., Steinhausen, C., Lamanna, G., Weigand, B., and Förster, F. J., *Fuel*, Vol. 233, 2018, pp. 918–925.
[8] Bork, B., Preusche, A., Weckenmann, F., Lamanna, G., and Dreizler, A., *Proceedings of the Combustion Institute*, Vol. 36, No. 2, 2017, pp. 2433–2440.
[9] Steinhausen, C., Lamanna, G., Weigand, B., Stierle, R., Groß, J., Preusche, A., and Dreizler, A., *Proceedings ILASS–Europe 2017. 28th Conference on Liquid Atomization and Spray Systems: 6-8 September 2017, Valencia, Spain*, 2017.
[10] Lamanna, G., Steinhausen, C., Weigand, B., Preusche, A., Bork, B., Dreizler, A., Stierle, R., and Groß, J., *International Communications in Heat and Mass Transfer*, Vol. 98, 2018, pp. 49–58.
[11] Santoro, M. and Gorelli, F. A., *Physical Review B*, Vol. 77, No. 21, 2008.
[12] Simeoni, G. G., Bryk, T., Gorelli, F. A., Krisch, M., Ruocco, G., Santoro, M., and Scopigno, T., *Nature Physics*, Vol. 6, No. 7, 2010, pp. 503–507.
[13] Bencivenga, F., Cunsolo, A., Krisch, M., Monaco, G., Ruocco, G., and Sette, F., *The Journal of chemical physics*, Vol. 130, No. 6, 2009, pp. 064501.
[14] Qiu, L. and Reitz, R. D., *International Journal of Multiphase Flow*, Vol. 72, 2015, pp. 24–38.
[15] Dahms, R. N., *Physics of Fluids*, Vol. 28, No. 4, 2016, pp. 042108.
[16] Bork, B. S., Dreizler, A., and Weigand, B., PhD-Thesis, Technische Universität Darmstadt, Darmstadt, 2017.
[17] Gross, J. and Sadowski, G., *Industrial & Engineering Chemistry Research*, Vol. 40, No. 4, 2001, pp. 1244–1260.
[18] Lemmon, E. W., Bell, I. H., Huber, M. L., and McLinden, M. O., 2018.
[19] Amagat, E. H., *Annales de chimie et de physique*, Vol. 19, No. 5, 1880, pp. 345–385.
[20] Wilke, C. R. and Lee, C. Y., *Industrial & Engineering Chemistry*, Vol. 47, No. 6, 1955, pp. 1253–1257.
[21] Luijten, C. C. M., PhD-Thesis, Technische Universiteit Eindhoven, Eindhoven, 1998.
[22] Rieber, M., Graf, F., Hase, M., Roth, N., and Weigand, B., *Proceedings ILASS-Europe*, Sept. 2000, pp. 1–6.
[23] Gomaa, H., Stotz, I., Sievers, M., Lamanna, G., and Weigand, B., *ILASS â€“ Europe 2011, 24th European Conference on Liquid Atomization and Spray Systems, Estoril, Portugal, September 2011*, 2011.
[24] Roth, N. and. Schlottke, J., Urban, J., and Weigand, B., *ILASS*, Sept. 2008, pp. 1–7.
[25] Roth, N., Gomaa, H., and Weigand, B., *Proc. DIPSI Workshop 2010 on Droplet Impact Phenomena & Spray Investigation*, Bergamo, 2010.
[26] Hase, M. and Weigand, B., *ICHMT International Symposium on Advances in Computational Heat Transfer*, April 2004, pp. 1–23.
[27] Schlottke, J., Rauschenberger, P., Weigand, B., Ma, C., and Bothe, D., *ILASS - Europe 2011, 24th European Conference on Liquid Atomization and Spray Systems, Estoril, Portugal*, 2011.
[28] Ruberto, S., Reutzsch, J., Roth, N., and Weigand, B., *Experiments in Fluids*, Vol. 58, No. 5, 2017, pp. 55.
[29] Reutzsch, J., Ertl, M., Baggio, M., Seck, A., and Weigand, B., chap. Towards a Direct Numerical Simulation of Primary Jet Breakup with Evaporation, Springer International Publishing, 2019.
[30] Rauschenberger, P. and Weigand, B., *Journal of Computational Physics*, Vol. 282, 2015, pp. 98–112.
[31] Eisenschmidt, K., Ertl, M., Gomaa, H., Kieffer-Roth, C., Meister, C., Rauschenberger, P., Reitzle, M., Schlottke, K., and Weigand, B., *Journal of Applied Mathematics and Computation*, Vol. 272, No. 2, 1 2016, pp. 508–517.
[32] Harlow, F. H. and Welch, J. E., *Physics of Fluids*, Vol. 8, No. 12, 1965, pp. 2182–2189.
[33] Lafaurie, B., Nardone, C., Scardovelli, R., Zaleski, S., and Zanetti, G., *Journal of Computational Physics*, Vol. 113, No. 1, July 1994, pp. 134–147.
[34] Brackbill, J. U., Kothe, D. B., and Zemach, C., *Journal of Computational Physics*, Vol. 100, No. 2, June 1992, pp. 335–354.
[35] Popinet, S., *Journal of Computational Physics*, Vol. 228, No. 16, Sept. 2009, pp. 5838–5866.
[36] Hirt, C. W. and Nichols, B. D., *Journal of Computational Physics*, Vol. 39, No. 1, Jan. 1981, pp. 201–225.
[37] Schlottke, J. and Weigand, B., *Journal of Computational Physics*, Vol. 227, No. 10, May 2008, pp. 5215–5237.